J Biol Inorg Chem (2002) 7: 632–639
DOI 10.1007/s00775-002-0342-6

ORIGINAL ARTICLE

G. Matthias Ullmann · Louis Noodleman
David A. Case

Density functional calculation of pK_a values and redox potentials in the bovine Rieske iron-sulfur protein

Received: 14 August 2001 / Accepted: 19 December 2001 / Published online: 20 February 2002

Abstract The redox potential of the Rieske iron-sulfur protein depends on pH. It has been proposed that the histidines coordinating one of the irons are responsible for this pH dependence, but an experimental proof for this proposal is still lacking. In this work, we present a density functional/continuum electrostatics calculation of the pK_a values of the histidines in the Rieske iron-sulfur center. The calculated apparent pK_a values are 6.9 and 8.8 in the oxidized state, which are in good agreement with the corresponding experimental values of 7.5 and 9.2 and the measured pH dependence of the redox potential. Neither of these two pK_a values can, however, be assigned to only one of the histidines. We find that both histidines titrate over a wide pH range in the oxidized state. Reduction of the iron-sulfur center shifts the pK_a values to 11.3 and 12.8, thus above 10.0 as found experimentally. The results provide a complete picture of the coupling of proton and electron binding, showing strongly cooperative binding of protons at electrode potentials near the redox midpoint potential of the cluster. The potential biological function of the low pK_a value of the histidines and the shift upon reduction are briefly discussed. Electronic supplementary material to this paper (comprising tables with the partial charges of the Rieske iron-sulfur cluster, optimized geometries of the 12 different states, and p$K_{1/2}$ values for the non-coordinating residues of the Rieske protein in the oxidized and reduced state) can be obtained by using the Springer Link server located at http://dx.doi.org/10.1007/s00775-002-0342-6.

Keywords Density functional calculation · Rieske protein · Iron-sulfur protein · pK_a values · Redox potentials

Electronic supplementary material to this paper (comprising tables with the partial charges of the Rieske iron-sulfur cluster, optimized geometries of the 12 different states, and p$K_{1/2}$ values for the non-coordinating residues of the Rieske protein in the oxidized and reduced state) can be obtained by using the Springer Link server located at http://dx.doi.org/10.1007/s00775-002-0342-6

G.M. Ullmann · L. Noodleman · D.A. Case (✉)
Department of Molecular Biology,
The Scripps Research Institute,
10550 N. Torrey Pines Road, TPC-15, La Jolla,
CA 92037, USA
E-mail: case@scripps.edu
Fax: +1-858-7848896

Present address: G.M. Ullmann
IWR – Biocomputing, Universität Heidelberg,
Im Neuenheimer Feld 368, 69120 Heidelberg, Germany

Introduction

The cytochrome bc_1 complex is found in electron transfer chains in mitochondria and bacteria; related b_6f complexes are found in chloroplasts and algae. This family of *bc* complexes all contain two heme *b* centers, a high-potential heme center (either heme c_1 or *f*) and a Rieske iron-sulfur protein [1, 2]. The bc_1 complex oxidizes ubiquinol in a step that is coupled to proton translocation through the Q-cycle [2]. The *bc* complexes are important elements in respiration and photosynthesis, and the oxidation of the quinol by the Rieske protein is a key event, because the electron transfer bifurcates at this step, with one electron of the quinol going to the Rieske protein, the other to a *b*-form heme.

The redox potential of the Rieske iron-sulfur protein in *bc*-type cytochromes is much more positive than values typical for 2Fe-ferredoxins, and depends on pH [3, 4, 5, 6]. It has been speculated that the histidine residues coordinating to one of the irons are responsible for this pH dependence [3, 4, 5, 6]. An experimental proof for this hypothesis is, however, still lacking. Because of the paramagnetic nature of the Rieske iron-sulfur complex, an experimental determination of the pK_a values is not trivial. By quantum chemical methods it is possible to compute pK_a values to a high degree of accuracy [7, 8, 9]. Therefore, theoretical investigations can help to clarify whether the histidine residues are responsible for the measured pH dependence of the

redox potential or not, and how electron transfer and proton transfer events are coupled in this system. Here, we demonstrate that density functional calculations can provide a good account of the pH dependence of the redox potential for a Rieske-type iron-sulfur center, and a reasonable (but not perfect) value for the absolute redox potential. The results suggest that the histidines are indeed responsible for the pH dependence, but that the two observed inflection points in the pH profile should not be identified with individual histidine residues; rather, protonation of the two sites are strongly coupled to each other.

The Rieske iron-sulfur protein is a component of cytochrome bc_1 and contains an Fe_2S_2 cluster coordinated by two cysteine and two histidine residues [10]. Both histidine residues coordinate the iron with their $N_{\delta 1}$. The two irons are ferric and antiferromagnetically coupled in the oxidized form. A high-resolution structure of the Rieske fragment from bovine cytochrome bc_1 cleaved from its membrane anchor has been solved [11]. In the crystal structures of whole cytochrome bc_1, the part of the Rieske iron-sulfur protein that was crystallized as a fragment was found in different orientations in different structures [12, 13, 14], indicating a remarkable mobility of this protein. The mobility of the Rieske protein is connected to a hinge motion between the transmembrane helix and the crystallized fragment of the Rieske iron-sulfur protein. In some of the structures of cytochrome bc_1 the iron ligand His161 makes a hydrogen bond with the ubiquinol analogue stigmatellin [12, 14]. It is therefore likely that His161 also makes a hydrogen bond with ubiquinol during the catalytic reaction. This hydrogen bond is possibly involved in a coupled proton-electron transfer from the fully reduced quinol to the oxidized Rieske iron-sulfur cluster [2]. If this hypothesis is true, His161 must titrate in the physiological pH range in the oxidized form of the Rieske protein.

In this paper, we combine density functional and electrostatic calculations to compute the pK_a values of the histidines coordinating one of the two irons in the Rieske iron-sulfur center. First, we give the computational details and briefly explain the method that is used for computing the microscopic and macroscopic pK_a values. We apply this method first to methylimidazole and obtain reasonable agreement with experimental data to validate the method. Then, we apply this method to the Rieske iron-sulfur center.

Computational methods

Overview

The calculations reported here combine, for the first time, a set of techniques for looking at coupled proton and electron transfer in metalloenzymes. The energies and geometries of the active site cluster, with various numbers of electrons and protons bound, are estimated using density functional theory (DFT). The effect of the protein and solvent environment is incorporated using a continuum solvent model and a dielectric region with embedded charges to represent the protein. Once the energies of the relevant protonation and redox states are available, a statistical (Boltzmann) calculation is used to evaluate state populations for given values of temperature, pH, and solution redox potential. Equivalently, the partition function (or binding polynomial) for binding of protons can be factorized to interpret proton uptake or release in terms of "apparent" pK_a values. Details of the individual pieces of this scheme are given in the following paragraphs.

Quantum chemical and electrostatic calculations

The Rieske protein can be proteolytically cleaved from its membrane anchor and the fragment has properties comparable to the Rieske protein in the intact cytochrome bc_1 complex. The structure of this fragment is known at 1.5 Å resolution [11] (PDB code 1RIE). This geometry was used as the starting structure for the calculation. Hydrogen-bond partners were also included in the quantum chemically treated model (see Fig. 1). The geometry was optimized with ADF 2000.02 [15] by density functional methods (functionals VWN [16] and PW91 [17]) and a high-level basis set (triple-ζ plus polarization – ADF Basis IV). The frozen core includes the (1s, 2s, 2p) orbitals of Fe and S, and the 1s orbitals of N, C, and O. We used the broken symmetry approach [18] to represent the antiferromagnetic coupling. We optimized a total of 12 states, corresponding to the four possible protonation states in the oxidized cluster and in the two reduced clusters. In the two reduced states, the electron is either placed at the iron coordinated by the histidine residues (by adding a spin-up electron) or at the iron coordinating the cysteines (by adding a down-spin electron; see Fig. 1 for spin vectors). The following atoms were fixed during the minimization: the peptide N and carbonyl C of His141, the peptide N and carbonyl C of His161, C_β of Cys139, C_β of Cys158, the carbonyl C of Thr140, the carbonyl C of Pro159, the peptide N of Leu142, C_β of Ser163, and C_ζ of Tyr165. Point charges obtained by fitting the quantum electrostatic potential using a CHELPG algorithm [19] combined with singular value decomposition [20] were used to estimate the interaction energy of the Rieske center with the protein and solvent environment [21] by solving the Poisson-Boltzmann equation numerically using MEAD 1.1.8 [22]. The following radii have been used for the charge fit and the solvation energy calculations: Fe 1.3 Å, N 1.55 Å, C 1.7 Å, O 1.5 Å, S 1.8 Å, and H 1.2 Å. Partial charges from CHARMM22 [23] and radii published by Bondi [24] were used for the protein. The system was divided into three dielectric regions: $\epsilon = 1$ for the quantum-chemically treated cluster, $\epsilon = 4$ for the protein, and $\epsilon = 80$ for water [21]. These parameters are reasonable from physical considerations [21, 25] and gave good agreement with experimental results in previous calculations [26, 27, 28, 29, 30]. In the quantum-chemically treated cluster, all degrees of freedom are treated explicitly, i.e. no additional shielding is required; thus the dielectric in this region is 1.0. In the protein, the electronic degrees of freedom and nuclear rearrangements are not considered explicitly. They are considered with a dielectric constant of 4.0. The ionic strength in the calculation of the pK_a values of the Rieske center was set to 0.15 M, which is equivalent to the physiological ionic strength. In the calculation of the pK_a values of methylimidazole (a model for histidine), the ionic strength was set to zero according to the experimental conditions. The optimized geometries and point charges are given in the Supplementary material.

Titration of non-coordinating residues by a continuum electrostatic method

We calculated the protonation probability for the Rieske protein by a standard method [22, 25, 37] using the numerical solution of the Poisson-Boltzmann equation to calculate protonation and interaction energies and Monte Carlo simulation for protonation state sampling. The Poisson-Boltzmann equation was solved with the program MEAD [22]. The Monte Carlo sampling was done

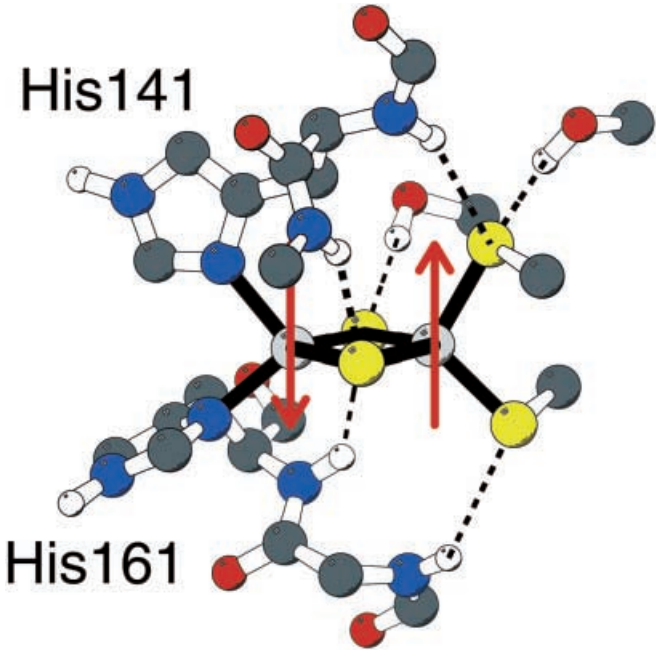

Fig. 1. Structure of the center used in the quantum chemical calculation. Non-polar hydrogens are omitted for clarity. The antiferromagnetic spin-coupling between the two iron centers is shown by the *red arrows*

with the program Karlsberg [30]. The protonation probabilities were calculated for the oxidized and reduced states of the Rieske center. The coordinating histidines were always protonated in these calculations. These calculations were done to see whether the redox state of the Rieske center influences the protonation probability of any residue in the Rieske protein.

Calculation of the protonation and redox equilibrium constants and protonation and reduction probabilities

The microscopic protonation and redox equilibrium constants between the different states of the metal cluster were calculated by a method [21, 27] which was described in more detail previously. The microscopic pK_a values were obtained from the thermodynamic cycle depicted in Fig. 2 using the following equations. The pK_a values relate directly to the free energy of deprotonation in aqueous solution, $\Delta G^{\text{deprot}}_{\text{water}}$, by Eq. 1. $\Delta G^{\text{deprot}}_{\text{water}}$ can be expressed as a sum of two contributions: the solvation energy difference $\Delta\Delta G^{\text{deprot}}_{\text{vac}}$ between the associated and dissociated system and the gas phase deprotonation energy $\Delta G^{\text{deprot}}_{\text{solv}}$:

$$pK_a = \frac{1}{\ln\ 10\ k_B T}\Delta G^{\text{deprot}}_{\text{water}} = \frac{1}{\ln\ 10\ k_B T}\left(\Delta G^{\text{deprot}}_{\text{vac}} + \Delta\Delta G^{\text{deprot}}_{\text{solv}}\right) \quad (1)$$

The solvation energy difference $\Delta\Delta G^{\text{deprot}}_{\text{solv}}$ is obtained from Eq. 2:

$$\Delta\Delta G^{\text{deprot}}_{\text{solv}} = \Delta G_{\text{solv}}(A^-) + \Delta G_{\text{solv}}(H^+) - \Delta G_{\text{solv}}(AH) \quad (2)$$

The solvation energy of the protonated and deprotonated molecule, $\Delta G_{\text{solv}}(A^-)$ and $\Delta G_{\text{solv}}(AH)$, was calculated by solving the Poisson-Boltzmann equation using the program MEAD as described above. The solvation energy of a proton, $\Delta G_{\text{solv}}(H^+)$, was set to –260.5 kcal/mol, as can be calculated from the experimentally measured potential of the standard hydrogen electrode [31]. The calculated pK_a depends linearly on the choice of the solvation energy of a proton, as can be seen from Eq. 2. The gas phase protonation energy was $\Delta G^{\text{deprot}}_{\text{vac}}$, calculated from Eq. 3:

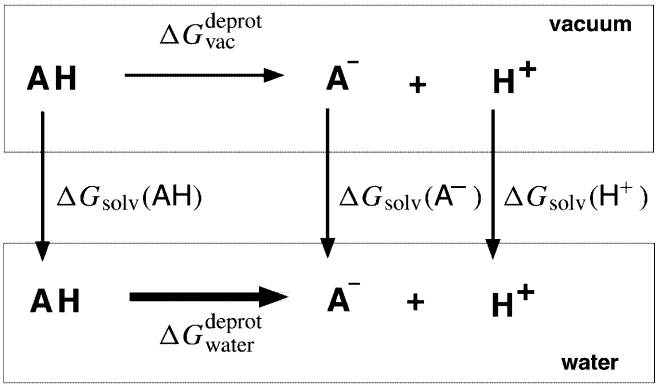

Fig. 2. Thermodynamic cycle to calculate absolute pK_a values. Instead of calculating free energy of dissociation of a proton from an acid in water ($\Delta G^{\text{deprot}}_{\text{water}}$) directly, the free energy of dissociation is first calculated in vacuum and the reactant and products are then transferred from vacuum into water

$$\Delta G^{\text{deprot}}_{\text{vac}} = \Delta H^{\text{deprot}}_{\text{vac}} + \Delta H^{\text{deprot}}_{\text{vib}} + H_{\text{trans}}(H^+) + \Delta(pV) - T[S(H^+)] \quad (3)$$

where $\Delta H^{\text{deprot}}_{\text{vac}}$ is the difference in the vacuum energy of the associated (protonated) and dissociated (deprotonated and hydrogen ion) system as calculated from ADF; $\Delta H^{\text{deprot}}_{\text{vib}}$ is the change in the vibrational energy between the protonated and deprotonated state and was estimated from a normal mode analysis of methylimidazole to be –8.0 kcal/mol. The main contribution to this vibrational term is the zero-point energy of the N-H bond that is being lost upon deprotonation. Because of the large cost of doing a normal mode calculation on the full iron-sulfur cluster, we have used methylimidazole as a model compound, essentially assuming that the frequency of the N-H bond is not changed very much upon coordination to the iron. $H_{\text{trans}}(H^+)$ is the translational energy of a proton, which is $\frac{3}{2}k_B T$; $\Delta(pV)$ is the energy change due to the volume change in the gas phase reaction, which is estimated from ideal gas approximations to be $k_B T$; and $T[S(H^+)]$ is the entropic portion of the gas-phase free energy of a proton and was set to 7.8 kcal/mol as derived from the Sackur-Tetrode equation [32].

The redox potential E^0_{redox} is computed by a similar approach. However, we neglect the cluster/protein entropy difference between oxidized and reduced states. The redox potential E^0_{redox} is calculated from Eq. 4:

$$E^0_{\text{redox}} = \frac{1}{F}\left(\Delta H^{\text{redox}}_{\text{vac}} + \Delta\Delta G^{\text{redox}}_{\text{solv}}\right) + \Delta\text{SHE} \quad (4)$$

where $\Delta H^{\text{redox}}_{\text{vac}}$ is the difference in the vacuum energy between the oxidized and reduced state, $\Delta\Delta G^{\text{redox}}_{\text{solv}}$ is the difference in interaction energy with the protein and solvent between the oxidized and reduced state, F is the Faraday constant (23.06 kcal/mol), and ΔSHE is the standard potential of the hydrogen electrode (–4.43 V).

The protonation and reduction probabilities are calculated from the grand canonical partition function [32, 33]. The theoretical background is explained in more detail elsewhere [25, 34, 35]. The grand canonical partition function is here a function of two external variables representing the chemical potential of the electrons and the protons. The energy of each possible state is calculated from the microscopic redox potentials and pK_a values. A thermodynamic average over all the possible states coupled to the external chemical potential of the electrons and the protons leads to the plots displayed in Fig. 5.

The macroscopic or apparent pK_a values are obtained from the roots of the grand canonical partition function Z [33, 36], which is a polynomial in the ligand activity $\Lambda = 10^{-\text{pH}}$ (binding polynomial). The grand canonical partition function Z at the oxidized state is given by Eq. 5:

$$Z = 1 + \left(10^{-\mathrm{p}K_{11}^{\mathrm{ox}}} + 10^{-\mathrm{p}K_{21}^{\mathrm{ox}}}\right)\Lambda + 10^{-\mathrm{p}K_{11}^{\mathrm{ox}} - \mathrm{p}K_{12}^{\mathrm{ox}}}\Lambda^2 = 1 + \left(10^{-\mathrm{p}K_{11}^{\mathrm{ox}}} + 10^{-\mathrm{p}K_{21}^{\mathrm{ox}}}\right)\Lambda + 10^{-\mathrm{p}K_{21}^{\mathrm{ox}} - \mathrm{p}K_{22}^{\mathrm{ox}}}\Lambda^2 \quad (5)$$

where $\mathrm{p}K_{11}^{\mathrm{ox}}$ and $\mathrm{p}K_{21}^{\mathrm{ox}}$ are the microscopic $\mathrm{p}K_{\mathrm{a}}$ values for the first deprotonation step, and $\mathrm{p}K_{12}^{\mathrm{ox}}$ and $\mathrm{p}K_{22}^{\mathrm{ox}}$ are the microscopic $\mathrm{p}K_{\mathrm{a}}$ values for the second deprotonation step. In the reduced state, the grand canonical partition function is a bit more complex because the Rieske center can be reduced either at the iron coordinated by the histidines or at the iron coordinated by the cysteines. Therefore the grand canonical partition function for the reduced system in Eq. 6 has twice as many terms:

$$Z = 1 + 10^{\Delta G^{\mathrm{redox}}} + \left(10^{-\mathrm{p}K_{11}^{\mathrm{red1}}} + 10^{-\mathrm{p}K_{21}^{\mathrm{red1}}} + 10^{-\mathrm{p}K_{11}^{\mathrm{red2}} + \Delta G^{\mathrm{redox}}} + 10^{-\mathrm{p}K_{21}^{\mathrm{red2}} + \Delta G^{\mathrm{redox}}}\right)\Lambda + \left(10^{-\mathrm{p}K_{11}^{\mathrm{red1}} - \mathrm{p}K_{12}^{\mathrm{red1}}} + 10^{-\mathrm{p}K_{11}^{\mathrm{red1}} - \mathrm{p}K_{12}^{\mathrm{red2}} + \Delta G^{\mathrm{redox}}}\right)\Lambda^2$$
$$= 1 + 10^{\Delta G^{\mathrm{redox}}} + \left(10^{-\mathrm{p}K_{11}^{\mathrm{red1}}} + 10^{-\mathrm{p}K_{21}^{\mathrm{red1}}} + 10^{-\mathrm{p}K_{11}^{\mathrm{red2}} + \Delta G^{\mathrm{redox}}} + 10^{-\mathrm{p}K_{21}^{\mathrm{red2}} + \Delta G^{\mathrm{redox}}}\right)\Lambda + \left(10^{-\mathrm{p}K_{21}^{\mathrm{red1}} - \mathrm{p}K_{22}^{\mathrm{red1}}} + 10^{-\mathrm{p}K_{21}^{\mathrm{red2}} - \mathrm{p}K_{22}^{\mathrm{red2}} + \Delta G^{\mathrm{redox}}}\right)\Lambda^2 \quad (6)$$

where $\Delta G^{\mathrm{redox}}$ is the energy difference in $\mathrm{p}K_{\mathrm{a}}$ units between the reduced state of the Rieske center when it is reduced at the iron coordinated by the histidines and the reduced state of the Rieske center when it is reduced at the iron coordinated by the cysteines, and is given by Eq. 7:

$$\Delta G^{\mathrm{redox}} = -\frac{F}{\ln\ 10\ k_{\mathrm{B}}T}\left(E_2^{\mathrm{prot}} - E_1^{\mathrm{prot}}\right) \quad (7)$$

The apparent $\mathrm{p}K_{\mathrm{a}}$ values are then the negative of the logarithm of the negative of the roots $\Lambda_{1,2}$ of the grand canonical partition function Z, $\mathrm{p}K_{1,2}^{\mathrm{app}} = -\log\left(-\Lambda_{1,2}\right)$. The apparent $\mathrm{p}K_{\mathrm{a}}$ values correspond to the macroscopic $\mathrm{p}K_{\mathrm{a}}$ values of the system and usually cannot be assigned to particular group, but are a property of the whole system.

Results and discussion

Geometry of the different redox and protonation states

The geometry of the Rieske center changes only slightly upon optimization. The metal-metal and metal-ligand distances are listed in Table 1. The metal-ligand distances are about as sensitive to the protonation state of the complex as to the redox state. When the last histidine is protonated and the corresponding Fe site is reduced, the Fe-N bond changes from 1.99 Å in the totally deprotonated and oxidized state to 2.14 Å for His141 or 2.10 Å for His161 in the totally protonated and reduced state. In the oxidized, singly deprotonated state the Fe-N bond to the deprotonated (imidazolate-type) histidine is always shorter than the other neutral (protonated) histidine, comparing 1.97 Å to 2.10 Å. The variation of Fe-N distance with protonation of the histidine is considerably larger for Fe(III) than for Fe(II). These differences in bond lengths may be useful for comparison with future high-quality data for the oxidized Rieske, and for the comparison of Fe-N distances to protonated versus deprotonated histidines. Comparisons to the 1.5 Å crystal structure of a Rieske fragment [11] (which is probably in the fully protonated, reduced form) are shown in the final two columns of Table 1. The computed metal-ligand bond lengths are on average within 0.04 Å of those from the crystal structure, but our predicted metal-metal distance is about 0.1 Å shorter than that observed. A complete listing of all optimized geometries is given in the Supplementary material.

Titration of non-coordinating residues in the Rieske iron-sulfur protein

It is in principle possible that titratable residues in the protein other than the coordinating histidines are responsible for the pH-dependent redox potential. In particular, His164, Tyr157, and Tyr165 are all reasonably close to the iron-sulfur cluster. Hence, we computed the protonation probabilities of all titratable residues except the histidines of the iron-sulfur cluster for the oxidized and reduced states of the protein by a standard method [22, 25, 37]. This method was able in previous applications to reproduce and explain experimental results [26, 34, 38, 39], at least qualitatively. The protonation probabilities of all titratable groups show no significant dependence on the redox state of the

Table 1. Iron-iron and iron-ligand distances in the energy optimized geometries. The reduced geometry corresponds to the geometry in which the reducing electron is placed at the iron coordinated by the histidines. The distances are given in Å. X-ray values from [11]

	Doubly deprotonated		Singly deprotonated				Protonated		X-ray
	Oxid	Red	Oxid		Red		Oxid	Red	
			His141	His161	His141	His161			
Fe_{His}-Fe_{Cys}	2.67	2.68	2.63	2.62	2.61	2.59	2.61	2.58	2.71
Fe_{Cys}-S_1	2.18	2.20	2.20	2.19	2.21	2.19	2.17	2.21	2.24
Fe_{Cys}-S_2	2.19	2.19	2.18	2.18	2.20	2.20	2.20	2.20	2.24
Fe_{His}-S_1	2.26	2.27	2.20	2.18	2.22	2.22	2.20	2.19	2.24
Fe_{His}-S_2	2.22	2.31	2.22	2.22	2.26	2.25	2.17	2.22	2.24
Fe_{Cys}-S_{Cys139}	2.30	2.40	2.33	2.32	2.37	2.36	2.29	2.34	2.29
Fe_{Cys}-S_{Cys158}	2.35	2.37	2.26	2.27	2.31	2.30	2.25	2.29	2.22
Fe_{His}-N_{His141}	1.99	2.05	1.97	2.11	2.11	2.15	2.09	2.14	2.16
Fe_{His}-N_{His161}	1.99	2.06	2.10	1.97	2.13	2.06	2.09	2.10	2.13

Table 2. Calculated microscopic and macroscopic pK_a values of methylimidazole

Microscopic pK_a values[a]	
pK_{11}	7.1
pK_{21}	7.5
pK_{12}	11.7
pK_{22}	11.3
Apparent pK_a values	
pK_1^{app}	7.3
pK_2^{app}	12.3

[a]The meaning of the microscopic pK_a values is described in Fig. 3

iron-sulfur cluster. The so-called p$K_{1/2}$ values, i.e. the pH at which the protonation probability of a given residue is 1/2, are given for all protonatable residues in Table S3 of the Supplementary material. These p$K_{1/2}$ values indicate the titration behavior of non-coordinated sidechains do not appear to be strongly coupled to the redox state of the cluster. The largest coupling is for Tyr157, whose p$K_{1/2}$ changes by 0.6 pH units upon cluster reduction. From these calculations, we rule out that residues other than the histidines of the iron-sulfur cluster are responsible for the pH-dependent redox potential.

Calculation of the absolute pK_a values of methylimidazole

The side chain of histidine has two macroscopic pK_a values, 7.0 and 14.0. Microscopic pK_a values for the first deprotonation reaction have been estimated from measurements at *N*-methylated methylimidazoles [40] and were found to be 7.0 for the $N_{\delta 1}$ nitrogen and 6.6 for $N_{\epsilon 2}$ nitrogen. In order to evaluate the above-described method for computing absolute pK_a values, we applied it to free methylimidazole. The results are shown in Table 2 and in Fig. 3 and are in reasonable agreement with the experimental data. From Fig. 3b, one can see that both, $N_{\delta 1}$ and the $N_{\epsilon 2}$, are only partially protonated over a wide pH range.

Calculation of the absolute pK_a values of the coordinating histidines and redox potentials

Measurements of the pH dependence of the redox potential of the bovine Rieske protein fragment gave associated apparent pK_a values of 7.5 and 9.2 [4]. These values refer to the oxidized form of the Rieske protein. From the quantum chemical calculations, we obtained the microscopic pK_a values, which are listed in Table 3. The microscopic pK_a values cannot be directly compared to the experimentally measured apparent pK_a values. Macroscopic pK_a values can be derived from microscopic models by factorizing the binding polynomial [33, 36]. Applying statistical mechanics, one can also derive titration curves of the individual sites from the microscopic values [36]. The titration curves of

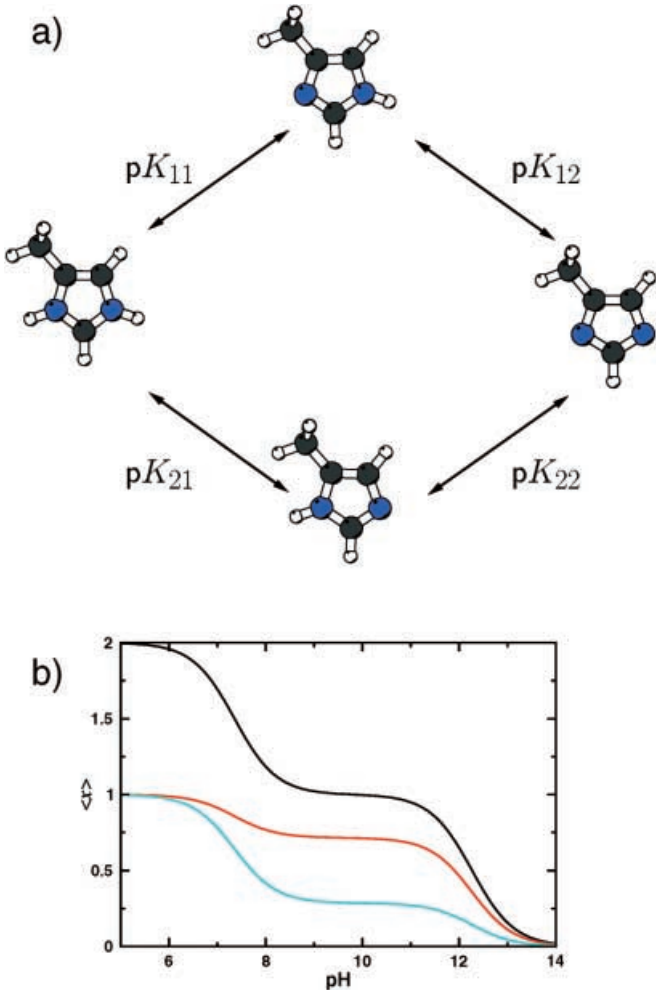

Fig. 3. **a** Scheme of the different protonation of methylimidazole. The scheme also marks the different microscopic pK_a values that are listed in Table 2. **b** Calculated titration curves of methylimidazole. The *black curve* represents the total protonation probability. The *red* and the *cyan curves* designate the titration curves of the $N_{\delta 1}$ and the $N_{\epsilon 2}$, respectively

His141 and His161 and the total titration curve of the cluster are shown for the oxidized and reduced state in Fig. 4. In the oxidized form, both histidines titrate over a wide pH range, and neither of the two residues can be assigned to just one of the apparent pK_a values. The sum of the two individual titration curves can, however, exactly be described as a sum of two standard titration curves having pK_a values of 6.9 and 8.8 and each site contributes to both of these pK_a values [36]. The calculated apparent pK_a values agree with the experimentally determined values [4]. In the reduced state, the electron is formally added to the iron which is ligated by the histidines. The reduction leads to higher electron density on these ligands, favoring the fully protonated form for both His141 and His161. According to our calculations, the pK_a values in the reduced state are shifted to 11.3 and 12.8, consistent with the experimental observation that the two histidines titrate above pH 10 [4].

Table 3. Calculated microscopic redox potential (protonated form) and microscopic and macroscopic pK_a values to describe the pH dependence of the redox potential of the Rieske center. The energy of each possible state of the Rieske center can be calculated by adding the different energy terms according to the scheme in Fig. 4

	Ox	Red (His)	Red (Cys)
Microscopic pK_a values[a]			
pK_{11}	7.1	11.3	8.9
pK_{21}	7.4	13.1	8.1
pK_{12}	8.6	13.4	9.0
pK_{22}	8.3	11.6	9.8
Microscopic redox potentials[b] (mV)			
E_1^{prot}			–12
E_2^{prot}			–390

	Ox	Red
Apparent pK_a values		
pK_1^{app}	6.9	11.3
pK_2^{app}	8.8	12.8

[a]The meaning of the microscopic pK_a values is described in Fig. 4
[b]The meaning of the microscopic redox potentials is described in Fig. 4

The calculated redox potential is –12 mV in the totally protonated form. The measured redox potential at low pH (pH 6) is 311 mV [4]. Previous calculations of absolute redox potentials of iron-sulfur clusters have also found values that are too low, by similar amounts [20, 21]. For example, calculations using the same methods we use here gave a redox potential for the ferredoxin from *Anabaena* 7120 that is 1.0 V more negative than the present result for the Rieske center [21]. Experimentally, this ferredoxin has a redox potential that is 0.75 V lower than a Rieske center. Differences in entropy between the oxidized and reduced states or changes in the protein geometry upon reduction, both of which are neglected here, are the most likely origins of these low estimates, although intrinsic errors in the DFT calculations themselves cannot be ruled out. Given the difficulties of calculating absolute redox potentials, we view the present result as acceptable.

Figure 5 shows the analytically calculated reduction probability and total protonation of the Rieske iron-sulfur cluster as a function of the external thermodynamic variables: the solution pH and electrode potential. A detailed theoretical framework of the method to compute these plots is given elsewhere [34, 35]. Although the calculated absolute redox potential is about 320 mV too negative, the dependence of the redox potential on pH is represented well by the calculation. The slope of the redox potential as a function of pH at pH 10 is –114 mV/pH and similar to the experimentally measured slope of –120 mV/pH at the same pH [4]. The fact that the absolute magnitude of the slope is greater than 60 mV/pH indicates that more than one proton is coupled to the redox event.

A common way to measure cooperativity is the Hill coefficient [41]. Hill coefficients larger than 1.0 indicate cooperative binding, those smaller than 1.0 indicate anti-

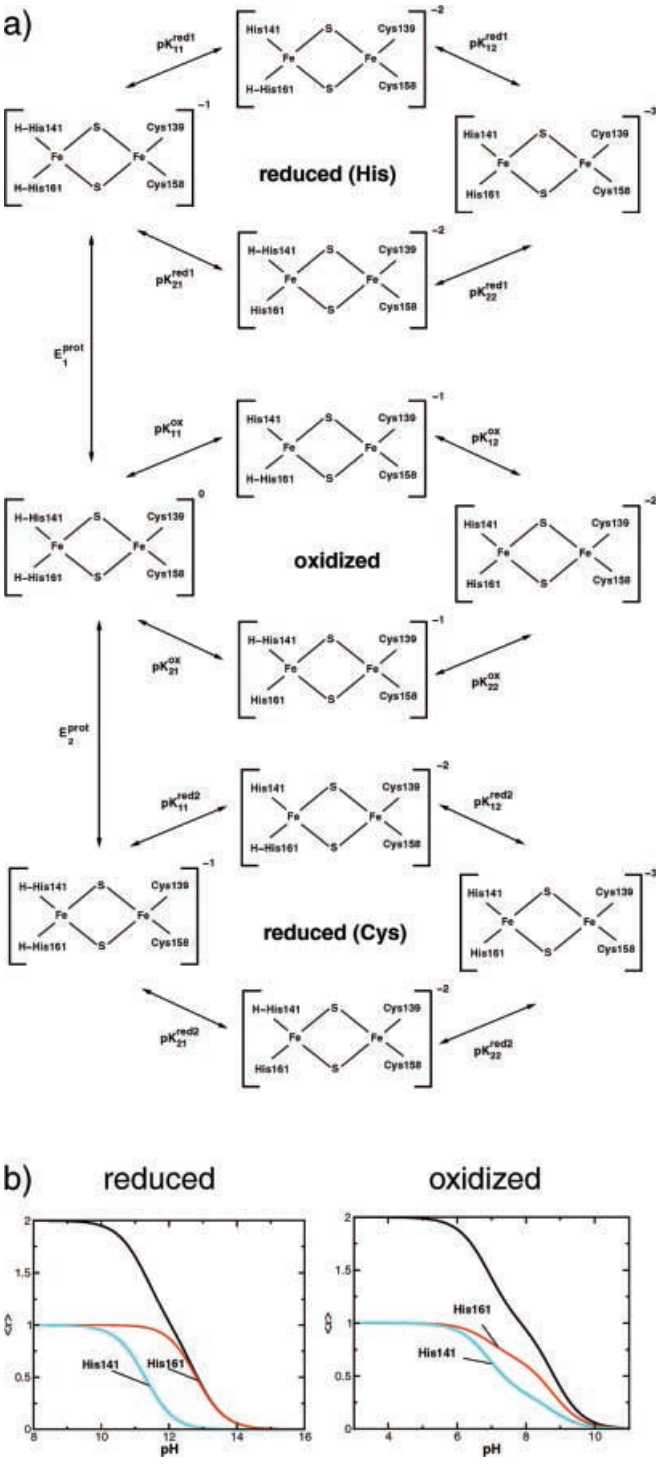

Fig. 4. **a** Scheme of the different protonation and redox states of the Rieske iron-sulfur protein. The scheme also marks the different microscopic pK_a values that are listed in Table 3. **b** Calculated titration of the histidines coordinating one iron in the Rieske iron-sulfur protein in the reduced (*left*) and oxidized (*right*) states. The *cyan* and the *red* curves designate His141 and His161, respectively. The *black curve* represents the total protonation probability of the iron-sulfur cluster and can be obtained as the sum of the cyan and the red curves

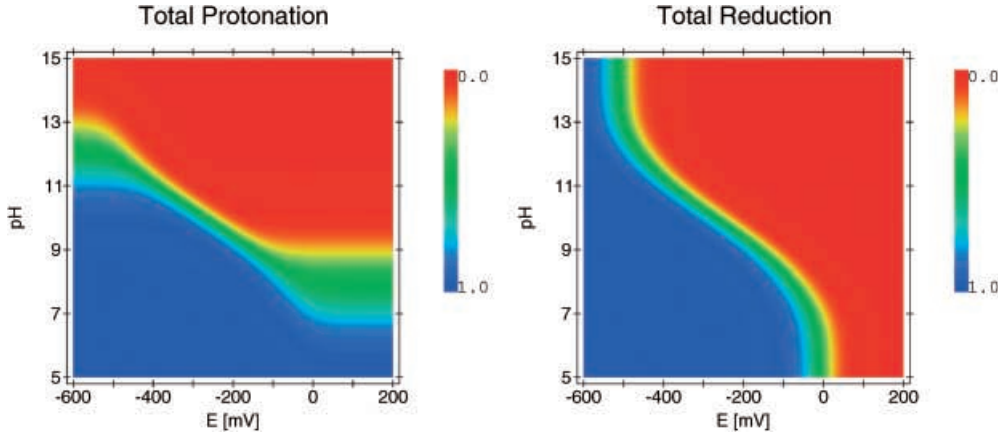

Fig. 5. Reduction probability and total protonation of the Rieske center in dependence on the electrode potential E (x-axis) and pH (y-axis). The z-axis represented by the color scheme reflects the probabilities. *Red* means totally deprotonated or totally oxidized, *blue* means totally protonated or totally reduced. The *green line* in the reduction probability plot represents the calculated redox potential as a function of pH. The left- and right-hand sides of the total protonation plot are equivalent to the black curves in the left- and right-hand sites in Fig. 4, respectively

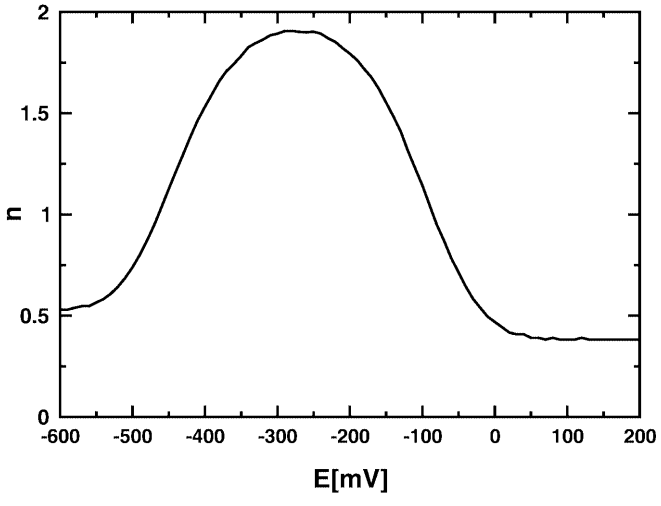

Fig. 6. Hill coefficient n for proton binding in dependence on the electrode potential E. We define the Hill coefficient as the derivative of the proton titration curve when one proton is bound to the system, i.e. the system is half protonated

cooperative binding or binding to independent sites with different binding constants. Figure 6 shows the Hill coefficient for protonation of the Rieske center as a function of solution redox potential. Cooperative proton binding occurs when the external electrode potential is near the redox potential of the Rieske cluster; at these electrode potentials, proton and electron binding are occurring simultaneously. At its maximum, the Hill coefficient nearly reaches 2, consistent with the large slope of the redox potential versus pH curve discussed above. At very high or very low electrode potentials (where the system is constrained to be either in the oxidized or reduced states), proton binding is anti-

Table 4. Energy difference between the reduced states when the electron is mainly localized at the iron coordinated by the histidine residues and the reduced state when the electron is mainly localized at the iron coordinated by the cysteine residues. ΔH^{red}_{gas} is the gas-phase energy difference between the two reduced states as calculated from ADF and $\Delta\Delta G^{red}_{solv}$ is the solvation energy difference calculated by using the Poisson-Boltzmann equation. The energy is given in kcal/mol

	ΔH^{redox}_{vac}	$\Delta\Delta G^{redox}_{solv}$	$\Delta H^{redox}_{vac} + \Delta\Delta G^{redox}_{solv}$
Protonated	–11.6	2.9	–8.7
Deprotonated His141	–6.0	1.6	–4.4
Deprotonated His161	–4.9	0.9	–4.0
Doubly deprotonated	0.6	–0.9	–0.3

cooperative, so that binding of a first proton inhibits binding of the second one.

Energetic difference between the reduction of two irons

In agreement with experiments [10], we find that the reducing electron is mainly localized at the iron coordinated by the histidine residues in the totally protonated state. Adding a down-spin electron (rather than an up-spin electron) as reducing electron to the oxidized Rieske center leads to the reduction of the iron coordinated by the cysteine residues (see Fig. 1 for the spin vectors). The energy of the configuration with the electron at the cysteine site is 8.7 kcal/mol higher than that of the configuration with the electron at the histidine site in the totally protonated form of the Rieske center. Thus the configuration with the electron at the cysteine site is thermally inaccessible in the protonated state. Deprotonating the histidines makes the two irons more equivalent. In the totally deprotonated form the difference between adding an electron to either the histidine or cysteine site is negligible, indicating that the two sites are nearly equivalent at very alkaline pH. The difference in energy between adding an electron to either the iron coordinated by histidines or to the iron coordinated by cysteines is listed in Table 4 (negative energies indicate that reduction at the histidine-bound iron is favored).

Conclusions

From our calculations, we can conclude that the two coordinated histidines are responsible for the pH dependence of the redox potential in the Rieske iron-sulfur center. The two pK_a values, however, cannot be assigned to particular histidines. Rather, both histidines titrate in the same pH range and both are thus partially responsible for both pK_a values. Since His161 titrates in the same range as His141 in the oxidized state, the postulated hydrogen bond between the fully reduced quinol and His161 of the oxidized Rieske iron-sulfur cluster [2] is entirely feasible. Rapid equilibration in the oxidized form between tautomers in which the proton is on either histidine would be expected.

The titration behavior of the two histidines has consequences for the mechanism of the ubiquinol reduction. In the oxidized state, both histidines have about the same protonation probability. According to our calculations, His161 has a higher affinity for protons than His141 after reduction. Thus a proton transfer from ubiquinol to the His161 will be faster than to His141 after reduction, according to Marcus theory [42, 43], if the transfer occurs in the normal region.

Overall, the calculations provide a good account of the proton-binding behavior, with computed pK_a values within 1 pH unit of those observed. Recent measurements on a Rieske fragment from *Thermus thermophilus* [44] provide apparent pK_a values for the oxidized cluster (7.8 and 9.6) that are similar to those seen in the bovine structure considered here, and also are able to see the reduced transitions (both at about pH 12.5), in good agreement with the values we report in Table 3. The absolute redox potential is computed to be too low, in accord with our previous experience using this method for iron-sulfur clusters [20, 21]. However, relative redox potentials, such as the difference in potential at high and low pH, are predicted quite accurately. We believe that these calculations provide additional evidence that these sorts of quantum investigations can be useful in the study of coupled proton/electron transfer in metalloenzymes.

Acknowledgements This work was supported by a postdoctoral fellowship of the Deutsche Forschungsgemeinschaft to G.M.U. (UL 174/1-1) and by NIH grant GM 39914. We thank Donald Bashford for providing his program MEAD, and E.J. Baerends and S. van Gisbergen for ADF.

References

1. Link TA (1997) FEBS Lett 412:257–264
2. Berry EA, Guergova-Kuras M, Huang L, Crofts AR (2000) Annu Rev Biochem 69:1005–1075
3. Prince RC, Dutton PL (1976) FEBS Lett 65:117–119
4. Link TA, Hagen WR, Pierik AJ, Assmann C, von Jagow G (1992) Eur J Biochem 208:685–691
5. Kuila D, Schoonover J, Dyer RB, Batie CJ, Ballou DP, Fee JA, Woodruff WH (1992) Biochim Biophys Acta 1140:175–183
6. Baymann F, Robertson DE, Dutton PL, Mäntele W (1999) Biochemistry 38:13188–13199
7. Chen JL, Noodleman L, Case D, Bashford D (1994) J Phys Chem 98:11059–11068
8. Richardson WH, Peng C, Bashford D, Noodleman L, Case DA (1997) Int J Quantum Chem 61:207–217
9. Topol IA, Tawa GJ, Burt SK, Rashin AA (1997) J Phys Chem A 101:10075–10081
10. Link TA (1999) Adv Inorg Chem 47:83–155
11. Iwata S, Saynovits M, Link TA, Michel H (1996) Structure 4:567–579
12. Zhang Z, Huang L, Shulmeister VM, Chi Y-I, Kim K-K, Hung L-W, Crofts AR, Berry EA, Kim S-H (1998) Nature 392:677–684
13. Iwata S, Lee JW, Okada K, Lee JK, Iwata M, Ramaswamy S, Link TA, Jap BK (1998) Science 281:64–71
14. Hunte C, Koepke J, Lange C, Rossmanith T, Michel H (2000) Structure 8:669–684
15. Guerra CF, Snijders JG, te Velde G, Baerends EJ (1998) Theor Chim Acta 99:391–403
16. Vosko SH, Wilk L, Nusair M (1980) Can J Phys 58:1200–1211
17. Perdew P, Chevary JA, Vosko SH, Jackson KA, Pederson MR, Singh DJ, Fiolhais C (1992) Phys Rev B 46:6671
18. Noodleman L, Baerends EJ (1984) J Am Chem Soc 106:2316–2327
19. Breneman CN, Wiberg KB (1990) J Comput Chem 11:361–373
20. Mouesca J-M, Chen JL, Noodleman L, Bashford D, Case DA (1994) J Am Chem Soc 116:11998–11914
21. Li J, Nelson MR, Peng CY, Bashford D, Noodleman L (1998) J Phys Chem A 102:6311–6324
22. Bashford D, Karplus M (1990) Biochemistry 29:10219–10225
23. MacKerell AD, Bashford D, Bellott M, Dunbrack RL Jr, Evanseck JD, Field MJ, Fischer S, Gao J, Guo H, Ha S, Joseph-McCarthy D, Kuchnir L, Kuczera K, Lau F, Mattos C, Michnick S, Ngo T, Nguyen DT, Prodhom B, Reiher WE, Roux B, Schlenkrich M, Smith JC, Stote R, Straub J, Watanabe M, Wiorkiewicz-Kuczera J, Yin D, Karplus M (1998) J Phys Chem B 102:3586–3616
24. Bondi A (1964) J Phys Chem 68:441
25. Ullmann GM, Knapp EW (1999) Eur Biophys J 28:533–551
26. Bashford D, Case DA, Dalvit C, Tennant L, Wright PE (1993) Biochemistry 32:8045–8056
27. Li J, Fischer CL, Chen JL, Bashford D, Noodleman L (1996) J Phys Chem 100:13498–13505
28. Li J, Fisher CL, Konecny R, Bashford D, Noodleman L (1999) Inorg Chem 38:929–939
29. Konecny R, Li J, Fisher CL, Dillet V, Bashford D, Noodleman L (1999) Inorg Chem 38:940–950
30. Rabenstein B, Ullmann GM, Knapp EW (2000) Biochemistry 39:10487–10496
31. Reiss H, Heller A (1985) J Phys Chem 89:4207–4213
32. Hill TL (1960) An introduction to statistical thermodynamics. Dover, New York
33. Wyman J, Gill SJ (1990) Binding and linkage. University Science Books, Mill Valley, Calif
34. Ullmann GM (2000) J Phys Chem B 104:6293–6301
35. Baptista AM, Martel PJ, Soares CM (1999) Biophys J 76: 2978–2998
36. Onufriev A, Case DA, Ullmann GM (2001) Biochemistry 40:3413–3419
37. Beroza P, Fredkin DR, Okamura MY, Feher G (1991) Proc Natl Acad Sci USA 88:5804–5808
38. Rabenstein B, Ullmann GM, Knapp EW (1998) Biochemistry 37:2488–2495
39. Kannt A, Lancaster C, Michel H (1998) Biophys J 74:708–721
40. Tanokura M (1983) Biochim Biophys Acta 742:576–585
41. Cantor CR, Schimmel PR (1980) Biophysical chemistry. Part III. The behaviour of biological macromolecules. Freeman, New York
42. Marcus RA, Sutin N (1985) Biochim Biophys Acta 811:265–322
43. Guthrie JP (1997) J Am Chem Soc 119:1151–1152
44. Zu Y, Fee JA, Hirst J (2001) J Am Chem Soc 123:9906–9907